ELECTRONIC SUPPLEMENTARY INFORMATION

Supplementary Figures

Figure S1. NMR biofilm reactor and electrodes. Top) The NMR biofilm reactor mounted on the custom NMR probe. The square copper Alderman-Grant-type resonator is shown surrounding the reactor door, on which the electrode is mounted. Green PEEK tubing influent lines, coming from the bottom, and effluent lines, coming from the top, allow for continual perfusion of the biofilm sample with growth medium. Bottom) Two example gold disc electrodes used to grow biofilms.

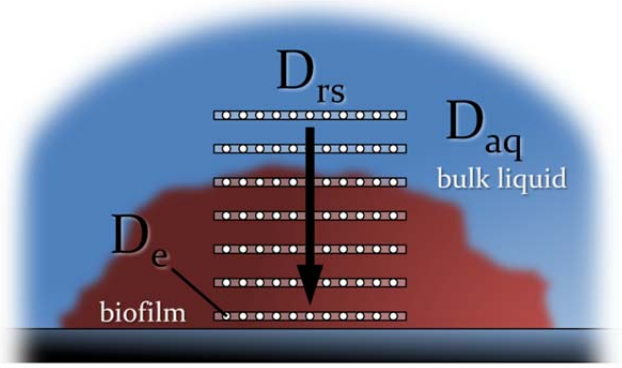

Figure S2. Diffusion coefficients in biofilm systems. Effective diffusion coefficients (D_e) are localized-volume measurements inside biofilms and take into account the hindered molecular diffusion rate caused by biofilm structure and porosity. D_e are smaller in magnitude than the free bulk liquid diffusion coefficient (D_{aq}). Surface-averaged relative effective diffusion coefficients (D_{rs}) are a specific type of D_e generated by averaging D_e by depth inside the biofilm and normalizing the results against D_{aq}. D_{rs} range from a value of 0 to 1, where 1 represents a D_{rs} that is equal to the D_{aq}. D_{rs} are defined mathematically by:

$$D_{rs} = \sum_{n=1}^{N} \frac{D_e(n)}{N \cdot D_{aq}}$$

where n is the arbitrary index for D_e values on a single plane parallel to the biofilm substratum and N is the total number of index values n on that plane. Figure S3 shows measurement voxels to scale for the D_e and D_{rs} measurements in this study.

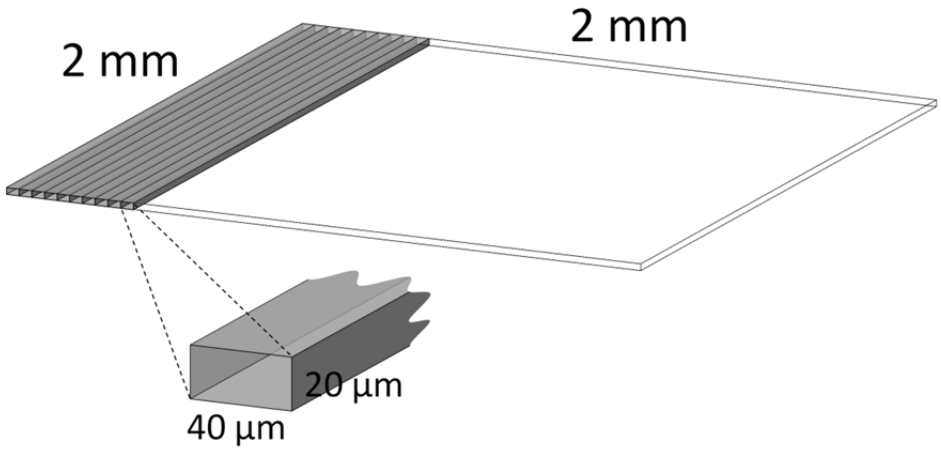

Figure S3. A single plane, parallel to the biofilm substratum, used to generate a D_{rs} data point in this study. This figure shows, to scale, 10 example D_e measurement voxels (40 µm × 20 µm × 2 mm) in relationship to the entire apparent D_{rs} measurement voxel (2 mm × 20 µm × 2 mm). Each D_{rs} data point is made by averaging 50 D_e values (50·40 µm = 2 mm). The depth resolution of D_{rs} measurements is 20 µm. This voxel is centered on the biofilm (concentric and parallel with the electrode) to avoid the biofilm edges and take measurements where the NMR signal is strong and magnetic field is more homogenous.

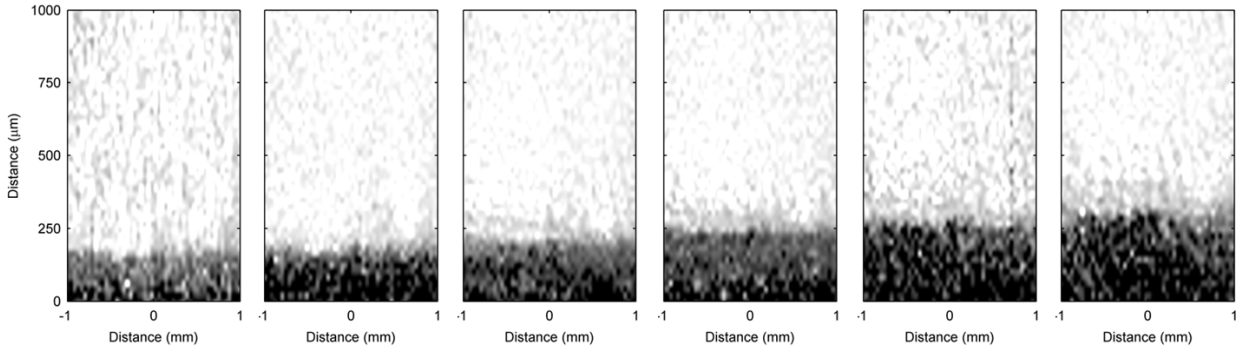

Figure S4. *G. sulfurreducens* biofilm growth. 2D relative D_e maps of a *G. sulfurreducens* biofilm and the NMR biofilm reactor obtained by PFG-NMR. The central 2 mm of the biofilm is shown. Each successive panel shows an increasingly older *G. sulfurreducens* biofilm. From left to right, the age is 24 days, 28 days, 33 days, 35 days, 47 days, and 52 days. Growth medium is pumped in the direction from -1 mm to +1 mm, parallel to the electrode.

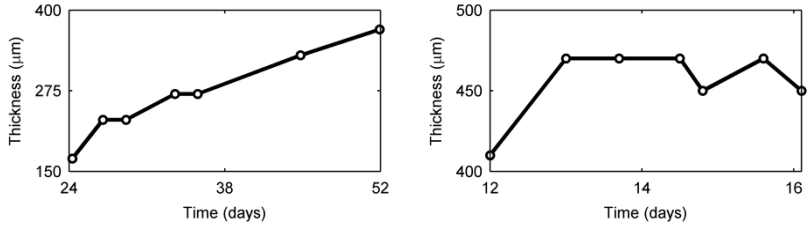

Figure S5. Biofilm thickness over time. Left) *Geobacter sulfurreducens*; Right) *Shewanella oneidensis*.

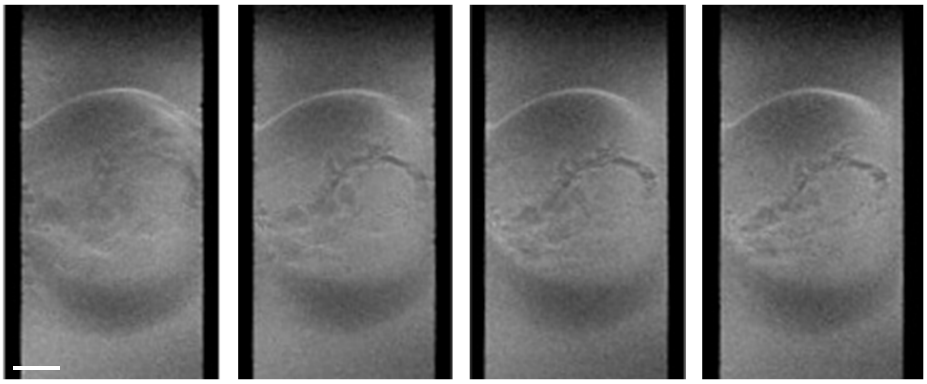

Figure S6. 2D MRI face-plane of *Shewanella* biofilm over time. Sequential face-plane 2D MRI of the biofilm, from 12 to 16 days old. The surface coverage of the biofilm decreases slightly over time. The channel is 4 mm wide. The white bar near the bottom of the first frame represents 1 mm.

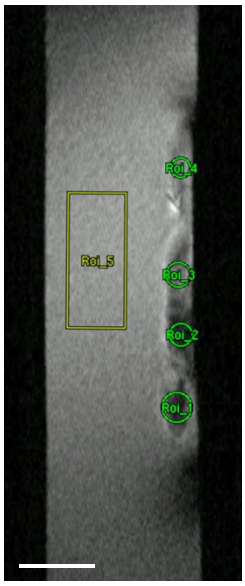

Figure S7. *S. oneidensis* biofilm cluster locations chosen for D_e measurements. Four clusters chosen to measure the average D_e, reported in Table 2. Roi_1, Roi_2, Roi_3, and Roi_4 correspond to Cluster 1, Cluster 2, Cluster 3, and Cluster 4, respectively. Roi_5 highlights the approximate region used in both the *S. oneidensis* and *G. sulfurreducens* experiments to determine the D_{aq} value. The white bar near the bottom represents 1 mm.

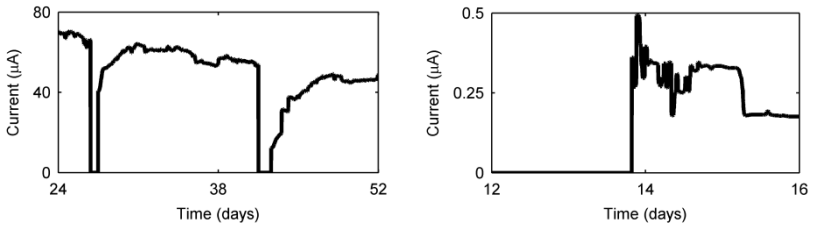

Figure S8. Biofilm current production over time. Left) *Geobacter sulfurreducens*; Right) *Shewanella oneidensis*. Current goes to zero during experiments when polarization is removed.

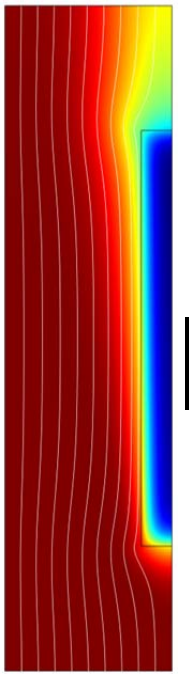

Figure S9. Two-dimensional model geometry. Nine white streamlines show the path of the assumed laminar fluid flow of the growth medium, which enters the channel at the bottom and is pumped against gravity. The biofilm is represented by a rectangular slab. The black scale bar near the bottom right corresponds to 1 mm. An example heat map shows the local acetate concentration in both the bulk liquid and in the biofilm, ranging from 20 mM (dark red) to 0 mM (dark blue).

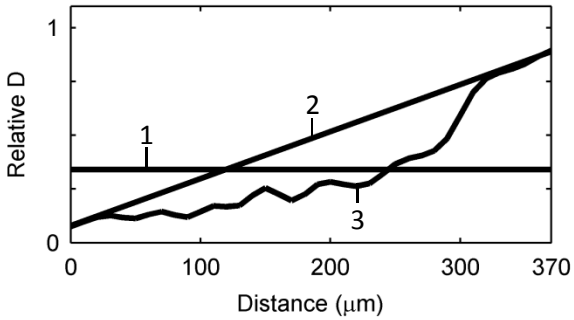

Figure S10. Three different D_e assumptions for the model: 1) a constant D_{rs} value, 2) a linearly decreasing D_{rs} profile, and 3) the true empirical profile. The constant D_{rs} chosen was identical to the average D_{rs} of the empirical data. Also, the minimum and maximum D_{rs} values in the linearly decreasing and empirical profiles were identical. The empirical data were taken from the measurements of the 52-day-old *G. sulfurreducens* biofilm shown in Figure 3.

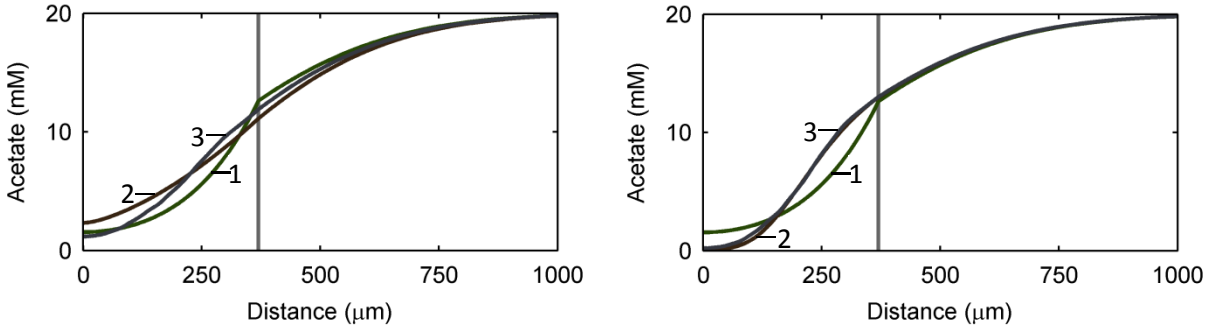

Figure S11. Simulated acetate concentration depth profiles. Acetate concentration profiles calculated for 1) a constant D_{rs} value (green), 2) a linearly decreasing D_{rs} profile (brown), and 3) the true empirical profile (dark blue). Left) Profiles assuming constant biofilm density. Right) Profiles assuming a biofilm density that was related to the D_{rs} using Equation 2.

Supplementary NMR Methods

2D Fourier transform MRI.

All 2D MRI data were collected using Bruker Paravision spin-echo method MSME. Face-plane (facing normal to the biofilm surface) 2DFT data employed field of view (FOV) dimensions of 10.24 mm by 5.12 mm. One hundred twenty-eight repetitions were collected with an echo and repetition time ratio (TE/TR) of 10.85/1000 milliseconds and 128 phase-encoding steps, for a total acquisition time of 4.5 hours. A total of 256 complex points were sampled at a rate of 200 Hz per pixel in the flow direction, with 128 phase-encoding steps in the lateral direction, for an in-plane resolution of 40 μm by 40 μm. The slice thickness was 3 mm. Normal-plane (facing parallel with the biofilm surface) 2DFT data employed field of view (FOV) dimensions of 10.24 mm by 5.120 mm. A total of 256 complex points were sampled at a rate of 200 Hz per pixel in the flow direction, with 256 phase-encoding steps in the biofilm-normal direction, for an in-plane resolution of 40 μm by 20 μm. The slice thickness was 2 mm. All 2DFT scans employed Hermite 90-degree excitation pulses (10 kHz pulse bandwidth) and Hermite 180-degree radio frequency (RF) pulses (8 kHz RF pulse bandwidth).

Diffusion-mapping 2D Fourier transform MRI.

Diffusion mapping employed Paravision method DtiStandard with a repetition time of 500 ms, an echo time of 16.665 ms, a total of 32 averages, a pulse gradient width (∂) of 3 ms, a diffusion time interval (Δ) of 10 ms, and 256 phase-encoding steps. The imaging sequence was repeated with seven different *b*-factors [0-1200 s/mm^2 in 200-s/mm^2 increments (diffusion-sensitive direction aligned normal to the biofilm surface)] for a total measurement time of ~8 hr. The *b*-factor is dependent on the timing and amplitude of the gradient pulses and the gyromagnetic ratio of the nucleus of detection (H^1). Renslow *et al*. (2010) describe in detail how the D_e maps and surface-averaged relative effective diffusion coefficient (D_{rs}) profiles were generated[55]. Briefly, two-dimensional diffusion maps were generated by processing the individual images (Gaussian noise filtering followed by fast 2DFT processing and saving the magnitude of each pixel), and then performing a semilogarithmic analysis (via the Bloch-Torrey equation) of the b-factor-dependent intensity values of each image pixel above a preset noise threshold using a custom-written MATLAB script. The center voxels of the 2D D_e maps (corresponding to the central 2mm by 2mm portion of the biofilm) were averaged to yield a depth-dependent D_{rs} profile with a resolution of 20 μm. The central 2mm by 2mm voxel location and size were used to ensure that measurements were taken where the magnetic field had the highest homogeneity and to avoid magnetic susceptibility discontinuities.

Supplementary Computational Modeling

Comsol Multiphysics (version number 4.2.1.166, COMSOL Inc., Burlington, MA, USA), a finite element method simulation package, was used to build and test the model. An 8-core, 64-bit Microsoft Windows 7 computer with 16 GB of RAM was used to run the simulation.

The model geometry was constructed to represent the NMR microimaging biofilm reactor, but was restricted to the area around the biofilm and NMR measurement voxel. The height of the reactor was set at 2 mm, and the length was set to 20% of the actual length (8 mm), centered on the biofilm. Modeling only the middle 8 mm of the reactor produced an identical fluid flow profile and acetate concentration in the NMR measurement voxel while reducing computational time. The inlet boundary condition for fluid flow was defined by Equation S1 to ensure that the fluid flow profile was laminar and matched the profile produced when a full-length reactor was simulated. Laminar flow was assumed because of the low Reynolds number of 0.1 for a flow of 1 mL/hr[55]. The *G. sulfurreducens* biofilm was assumed to be a 370-μm-thick rectangular slab positioned on the 5-mm electrode, utilizing a conductive electron transfer mechanism. Meshing of the two-dimensional domains (the NMR biofilm reactor and the biofilm) was performed using free triangular mesh elements, each with a maximum element size of 20 μm. Mesh elements along the center edge used to created depth profiles were constrained to a maximum element size of 1 μm in order to generate smooth depth profile plots and to ensure a high element density where the profiles would be produced.

The modeling parameters were identical to those of the experimental setup after the *G. sulfurreducens* biofilm had reached 370 μm thick, including fluid flow speed, inlet acetate concentration, and temperature. Acetate was fully oxidized in the biofilm assuming Nernst-Monod behavior, which is a specific case of multiplicative Monod behavior which accounts for the limitations of both the soluble electron donor (acetate) and the solid electron-accepting electrode[1]. The Nernst-Monod substrate utilization equation is given by:

$$q = q_{max}\left(\frac{S}{S+K_S}\right)\left(\frac{1}{1+e^{\left(-\frac{F}{RT}\left(E-E_{K_A}\right)\right)}}\right)$$

Equation S1

where q is the acetate substrate utilization rate (mmol/g·s), q_{max} is the maximum acetate substrate utilization rate (mmol/g·s), S is the concentration of acetate (mM), K_s is the half-saturation coefficient (mM), F is Faraday's constant (s·A/mol), R is the universal gas constant (J/K·mol), T is the temperature (K), E is the electrode polarization potential (V), and E_{K_A} is the half-maximum rate potential (V). However, for our case we ensured that the Nernst term (Equation S2) was ~1 by assuming a sufficiently positive electrode polarization potential:

$$\frac{1}{1+e^{\left(-\frac{F}{RT}\left(E-E_{K_A}\right)\right)}} \cong 1$$

Equation S2

This was done to match our experimental conditions and to ensure that the D_{rs} assumptions were the only cause for solution differences. The empirical D_{rs} profile in the biofilm was approximated by interpolating the data using piecewise cubic interpolation. Biofilm density was either assumed to be constant or was related to the D_{rs} using Equation 2. Acetate diffused following Fick's law and was consumed within the biofilm according to the Nernst-Monod substrate utilization equation. A steady-state mass balance for acetate is given by:

$$\frac{\partial S}{\partial t} = \nabla \cdot (D_{rs}\nabla S) - Xq = 0$$

Equation S3

Flux at the top of the biofilm, a parameter used to highlight the effects of different D_{rs} assumptions, was determined by averaging the flux of a 2 mm × 2 mm square surface located at the top 1 μm of the biofilm and concentric with the electrode. This region corresponded with the actual NMR measurement voxel used to generate the 2D D_{rs} maps. The total current produced by the biofilm was determined by integrating acetate flux over the projected volume of the biofilm to determine the total flux of acetate consumed by the biofilm and the electron equivalents generated.

Supplementary Discussion

Effect of temperature on D_{aq}

The D_{aq} in the *G. sulfurreducens* biofilm experiments was $2.82 \cdot 10^{-9}$ m^s/s (σ: $0.10 \cdot 10^{-9}$ m^s/s). This is slightly higher than the typical value for water at 30 °C [e.g., 5% higher than values reported by Beuling *et al*. (1998) and 17% higher than values reported by Renslow *et al*. (2010)]; however, diffusion coefficient values are known to be highly dependent on temperature[2-4].

Temperatures as high as 30.6 °C were recorded for the N_2 purge gas out of the bottom of the NMR probe, so it is likely that the NMR biofilm reactor experienced temperatures that were slightly higher than this because of the proximity of the reactor to the gas stream inlet. Interpolating from diffusion coefficient values given by Beuling *et al*. (1998), the reactor temperature should be around 31.7 °C to have a diffusion coefficient value of $2.82 \cdot 10^{-9}$ m^s/s. Furthermore, differences in growth medium composition can affect the D_{aq} of water. The D_{aq} in the *S. oneidensis* biofilm experiments was $2.49 \cdot 10^{-9}$ m^s/s (σ: $0.06 \cdot 10^{-9}$ m^s/s). Similar to the *G. sulfurreducens* experiment, this value is slightly higher than expected for water at 25 °C (8% higher than values reported by Beuling *et al*. (1998))[2]. Interpolating from values given by Beuling *et al*. (1998), the NMR biofilm reactor temperature may have been as high as 27.5 °C to measure a D_{aq} of $2.49 \cdot 10^{-9}$ m^s/s. Other possible causes of the elevated D_{aq} are the presence of background magnetic gradients in the NMR and less than ideal diffusion gradient pulses. The D_e results in the manuscript are reported as relative values so that the data are widely applicable for a wide range of temperatures used in EAB mathematical models and the exact cause for the slight elevation is not a concern.

Supplementary Works Cited

1. A. K. Marcus, C. I. Torres and B. E. Rittmann, *Biotechnol. Bioeng.*, 2007, **98**, 1171-1182.

2. E. E. Beuling, D. van Dusschoten, P. Lens, J. C. van den Heuvel, H. Van As and S. P. P. Ottengraf, *Biotechnol. Bioeng.*, 1998, **60**, 283-291.

3. R. S. Renslow, P. D. Majors, J. S. McLean, J. K. Fredrickson, B. Ahmed and H. Beyenal, *Biotechnol. Bioeng.*, 2010, **106**, 928-937.

4. J. Simpson and H. Carr, *Physical Review*, 1958, **111**, 1201.